CHAPTER-3

Halide perovskite-cobalt(III) complex photoredox catalyst for highly efficient N-Alkylation of amines with alcohols

3.1. Introduction

In Chapter 2, we discussed the role of the Ni-complex in facilitating the C–N coupling reaction via the H_2O_2 production pathway, specifically aiming to avoid water formation in the reaction mixture. Given the known instability of $CsPbBr_3$ under aqueous and moist conditions, this chapter focuses on the exploration of a Co-complex as a cocatalyst in combination with the $CsPbBr_3$ photocatalyst. Our goal is to achieve selective N-alkylation for amine synthesis through the hydrogen borrowing mechanism, while continuing to suppress water formation during the reaction.

Amines and nitrogen derivatives are vital in natural products, biologically active molecules, agrochemicals, drugs, and polymers.[1] N-alkylation of amines with alcohols offers a greener, milder, and more efficient alternative to traditional methods,[2–4] using cheap, accessible materials and producing only water.[5–8] The process involves alcohol dehydrogenation, imine formation, and imine hydrogenation via a borrowing hydrogen mechanism.[9–11]

The hydrogen atom transfer and borrowing hydrogen enable sustainable amine functionalization using alcohols as hydrogen donors, thereby avoiding the need for an external hydrogen source.[12] Since many alcohols come from renewables, this method supports biomass valorization. Previously, Beller, Balaraman, and Kempe groups explored homogeneous noble metal complexes like (Ru[13], Ir[14,15]) have been explored for N-alkylation reaction, but suffer from high cost, low stability, and recyclability. In this respect, heterogeneous catalysts offer durability and reuse but often lack activity, selectivity and require high temperatures.

Photoredox reactions using semiconductors offer a promising platform for the successful application to organic transformation reactions.[16] Recently, photoredox catalysis has proven to

be a valuable tool for organic synthesis, especially C−N coupling reactions, under mild conditions.[17,18] Zhang used CdS[1] with formic acid/formate for amine synthesis, while Li used Ni–Fe-MOF under visible light.[19] However, both relied on external hydrogen and showed poor selectivity and waste. Here, we explore photoredox N-alkylation of amines using alcohols without external hydrogen or high temperatures.

In this context, we demonstrate $CsPbBr_3$ QDs for N-alkylation of aniline with benzyl alcohol, yielding 24% conversion and 17% selectivity. Recently, cobaloxime was used as a hydrogen atom transfer mediator in organic transformations and the hydrogen evolution reaction (HER).[22–26] Adding a cobaloxime cocatalyst enhances activity, selectivity, and charge separation by mediating hydrogen atom transfer (HAT) and the hydrogen borrowing process for selective amine formation.[22,23,27] The Co centre aids hydrogen abstraction from alcohol and HAT to imine intermediates, forming N-benzylaniline. Ligand tuning at Co's equatorial sites modulates its electronic structure and catalytic performance.

In this chapter, the cobaloxime complex is presented with a CoN_4 skeleton as an ideal platform for organic transformations. Cobaloximes' intramolecular hydrogen bonding aids multi-hydrogen atom transformations, enhancing hydrogen atom delivery. Optoelectronic studies show that cobaloxime improves $CsPbBr_3$ QDs' charge separation and benzyl alcohol oxidation. The 2,3-diaminonaphthalen ligand in [Co-4] aligns well with the $CsPbBr_3$ conduction band. The π–π conjugation properties of [Co-4] enhance the photogenerated charge separation, and steric effects at the equatorial site facilitate hydrogen transfer. Combining $CsPbBr_3$ with cobaloximes ([Co-1], [Co-2], [Co-3], [Co-4]) boosts N-alkylation efficiency, with $CsPbBr_3$-[Co-4] achieving 97% selectivity and 98% conversion of aniline.

3.2. Chemicals

All the chemical details were mentioned in Chapter 2, Section 2.2.

3.3. Instruments

The same instruments described in Chapter 2, Section 2.3, were used for the spectroscopic, microscopic, and NMR characterization of the catalysts and products.

3.4. Experimental

3.4.1. Synthesis of $CsPbBr_3$ QDs

The $CsPbBr_3$ QDs synthesis methods mentioned in Chapter 2, Section 2.3, were followed.

3.4.2. Synthesis of oxime ligands and metal complexes (Co-1, Co-2, Co-3, and Co-4)

(i) Synthesis of Co-1 complex: Synthesis of the Co-1 complex was carried out following previously reported procedures, and the obtained ^1H NMR and ESI-MS data were consistent with literature values, all the ligand complexes and metal complexes mentioned in Figure 3.1.

(ii) Synthesis of Co-2 complex: Following a literature procedure with slight modifications, we first synthesized the L2 ligand, which was subsequently coordinated with $CoCl_2 \cdot 6H_2O$. The 606 mg 2,3-butanedione monoxime (6.00 mmol) was dissolved in 15 mL methanol, and 200 µL ethylenediamine (3.00 mmol) was rapidly added. The reaction mixture was stirred at room temperature, leading to the formation of a white solid after 2 hours. The solid was collected by filtration, washed with dichloromethane, and dried under vacuum to yield 400 mg of L2 ligand.

To synthesize Co-2 complex, 226 mg L2 ligand (1.00 mmol) and 238 mg of $CoCl_2 \cdot 6H_2O$ (1.00 mmol) were dissolved in 25 mL acetone and stirred at room temperature for 18 hours. The resulting yellow-green solid was filtered and washed with acetone.

(iii) Synthesis of Co-3 complex: To synthesise the L3 ligand, 606 mg 2,3-butanedione monoxime (6.00 mmol) and 324 mg 1,2-diaminobenzene (3.00 mmol) were dissolved in 15

mL distilled water and heated to reflux. An orange precipitate gradually formed after 5 hours. The reaction mixture was then cooled to 4 °C and left overnight. The resulting precipitate was collected by filtration, washed with cold water, and dried under vacuum to yield 394 mg of a brown solid.

For complexation, 274 mg of L3 ligand (1.00 mmol) and 238 mg of $CoCl_2 \cdot 6H_2O$ (1.00 mmol) were dissolved in 10 mL ethanol and refluxed for 4 hours. The reaction mixture was then subjected to crystallization using diethyl ether as the non-solvent, yielding a green solid.

(iv) Synthesis of Co-4 complex

The Co-4 was synthesized by reported literature modification **(Figure 3.1)**.[24] In synthesizing the $(DOH)_2Nap$ ligand, 606 mg 2,3-butanedione monoxime (6.00 mmol) and 324 mg 2,3-naphthalenediamine (3.00 mmol) were mixed in 5 mL water and heated at 80 ^oC to reflux for 10 h, a light brown precipitate formed, and then the mixture was cooled to 4 ^oC overnight. The precipitate was filtered, washed with cold water, and dried under a vacuum. Yield: 70%. ^1H NMR (500 MHz, DMSO-d6) δ 11.41 (s, 2H), 8.58 (dt, 2H), 8.18 (dt, J = 9.5 Hz, 2H), 7.60 (dd, J = 9.6 Hz, 2H), 2.72 (s, 6H), 1.92 (s, 6H). ^{13}C NMR (126 MHz, DMSO-d6) δ 155.74, 153.62, 137.96, 133.11, 128.71, 126.97, 126.31, 23.57, 9.87, which was consistent with the literature. ESI M^+ calculated 324.214.

The (L4) ligand (0.5 mmol) and $CoCl_2 \cdot 6H_2O$ (0.5 mmol) were mixed in 6 mL ethanol and refluxed for 6 h, and a green liquid was formed and extracted with ethyl acetate. ^1H NMR (500 MHz, DMSO-d6) δ 12.34 (s, 1H), 8.53 (dt, 2H), 8.14 (dd, J = 9.4 Hz, 2H), 7.57 (dt, J = 9.6 Hz, 2H), 2.26 (s, 6H), 1.77 (s, 6H). ^{13}C NMR (126 MHz, DMSO-d6) δ 197.41, 155.71, 137.87, 133.08, 128.67, 126.65, 126.28 – 126.23, 25.24, 8.25. Notably, the ligand complex and the metal complex were also confirmed by HR-MS and ESI M^+ calculated 453.169.

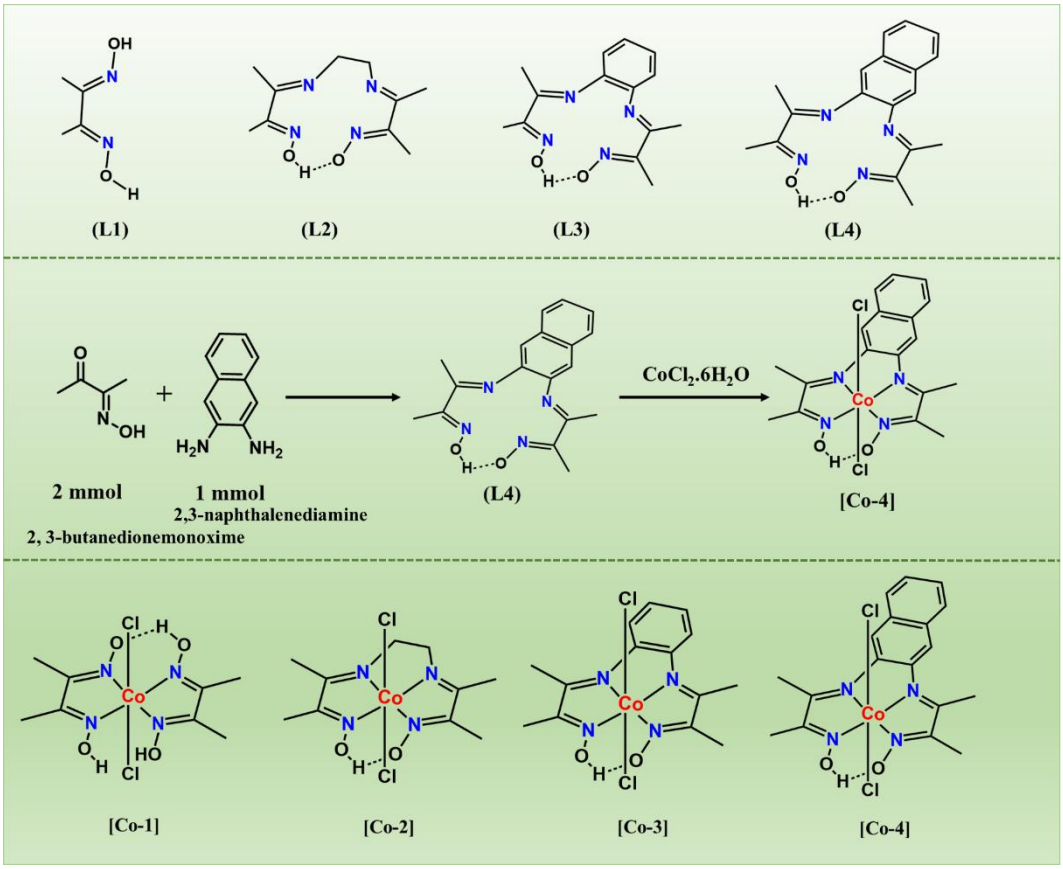

Figure 3.1. Molecular structures of ligands L1–L4, synthetic scheme of the [Co-4] complex, and the molecular structure of the resulting cobalt complex.

3.4.3. Preparation of [Co]-$CsPbBr_3$ catalysts

5 wt.% cobaloxime complexes (Co-1, Co-2, Co-3, and Co-4) concerning $CsPbBr_3$ QDs wt.% were dispersed in 3 mL toluene solution and stirred in the dark for 10 min to make a homogeneous suspension. Further, proceeded with the photocatalytic N-alkylation reaction. All 5 wt.% of cocatalysts (Co-1, Co-2, Co-3, and Co-4) were loaded with $CsPbBr_3$ solution as listed in **Table 3.1**.

3.5. Results and discussion

3.5.1. Characterizations of $CsPbBr_3$ QDs systems

All characterization data for $CsPbBr_3$ QDs, including PXRD, TEM, EDX, and XPS, are presented in Chapter 2, Section 2.6.[28-31]

Table 3.1. Description of the photocatalyst systems.

S.N.	Photocatalyst	Cocatalyst	Loading (wt.%)	Catalysts Code
1	$CsPbBr_3$	-	-	$CsPbBr_3$
2	$CsPbBr_3$	[Co-1]	5	$CsPbBr_3$-[Co-1]
3	$CsPbBr_3$	[Co-2]	5	$CsPbBr_3$-[Co-2]
4	$CsPbBr_3$	[Co-3]	5	$CsPbBr_3$-[Co-3]
5	$CsPbBr_3$	[Co-4]	5	$CsPbBr_3$-[Co-4]

3.6. Optical properties of the catalyst systems

UV-visible diffuse reflectance spectroscopy (DRS) of $CsPbBr_3$ QDs showed an absorption band at 518 nm, corresponding to a bandgap of 2.31 eV as calculated from the Tauc plot inset figure (**Figure 3.2a**). The incorporation of cocatalysts (Co-1, Co-2, Co-3, and Co-4) into $CsPbBr_3$ QDs did not alter the bandgap, and no distinct absorption peaks from the cocatalysts were observed due to their low concentrations. However, both the type of cocatalyst and its

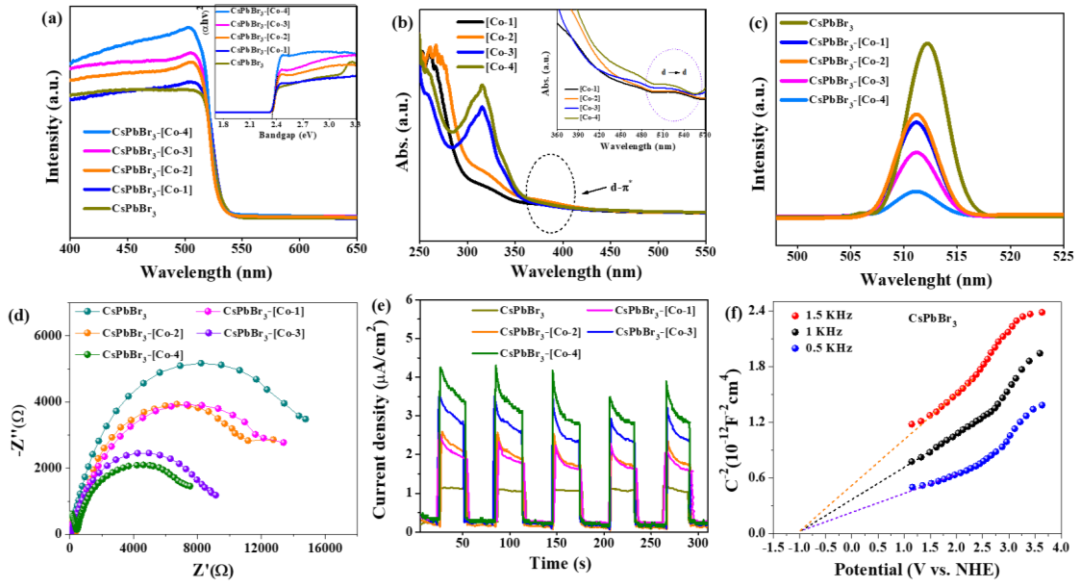

Figure 3.2. (a) The UV-DRS spectra of $CsPbBr_3$, $CsPbBr_3$-[Co-1], $CsPbBr_3$-[Co-2], $CsPbBr_3$-[Co-3], and $CsPbBr_3$-[Co-4], and the inset figure Tauc plot of all catalysts. (b) UV-visible spectra of the cocatalysts. (c) Photoluminescence spectra of $CsPbBr_3$ and others with cocatalysts. (d) Electrochemical impedance spectroscopic studies of bare $CsPbBr_3$ and with all the cocatalysts. (e) Photocurrent measurements of bare $CsPbBr_3$ and with all the cocatalysts under light/dark conditions. (f) Mott–Schottky measurements.

loading, specifically 3, 5, and 7 wt.% of Co-4, significantly influenced the photocatalytic performance in the N-alkylation reaction (**Table 3.2; see later discussion**). Additionally, UV-visible spectroscopy of [Co-4] displayed characteristic (d–d) and (d–π*) transitions at 520 nm and 380 nm, respectively (**Figure 3.2b**).[24,33–35] Notably, [Co-3] and [Co-4] exhibited stronger peak intensities compared to other complexes, suggesting more efficient charge transfer, inset **Figure 3.2b**.

3.7. Role of cocatalyst on charge transfer properties of $CsPbBr_3$ QDs

Photoluminescence (PL) spectroscopy of $CsPbBr_3$ QDs showed a characteristic emission peak at 519 nm, indicating their photogenerated charge separation properties (**Figure 3.2c**).[36] Upon introduction of cobaloxime cocatalysts, the PL intensity decreased, suggesting enhanced charge separation due to electron transfer from the CB of $CsPbBr_3$ QDs to the LUMO of the cocatalysts. Among them, [Co-4] exhibited the most significant quenching effect, corresponding to the highest degree of charge separation. This enhanced performance is attributed to strong π-acceptor conjugation within the [Co-4] ligand backbone, which facilitates efficient electron transfer and suppresses charge recombination. The observed trend in PL quenching correlates with the photocatalytic efficiency in the N-alkylation reaction, with [Co-4] delivering the highest activity (**Table 3.2**).

Electrochemical impedance spectroscopy (EIS) was employed to further investigate the photogenerated charge transport processes.[28] Nyquist plots revealed a significantly lower charge-transfer resistance for the $CsPbBr_3$-[Co-4] system compared to pristine $CsPbBr_3$ and other cocatalyst combinations ($CsPbBr_3$-[Co-1], $CsPbBr_3$-[Co-2], and $CsPbBr_3$-[Co-3]) (**Figure 3.2d**).

Additionally, photocurrent measurements under light on/off cycles demonstrated the

photogenerated charge transfer behavior of the catalysts (**Figure 3.2e**).[37] Among all samples, $CsPbBr_3$-[Co-4] exhibited the highest photocurrent, indicating the most efficient charge transport. This enhanced performance is attributed to the electron-deficient cobalt center in [Co-4], induced by its ligand environment, which facilitates electron transfer from the conduction band of $CsPbBr_3$ to the cocatalyst, thereby enhancing charge separation. These efficient charge transport characteristics directly contribute to improved photocatalytic activity and selectivity in the N-alkylation reaction. Collectively, the characterization results confirm that $CsPbBr_3$-[Co-4] exhibits superior charge separation and transfer properties, accounting for its enhanced photocatalytic performance.

The Mott–Schottky (MS) analysis of $CsPbBr_3$ revealed positive slopes in the frequency range of 0.5–1.5 kHz, confirming their n-type semiconductor behavior.[38] From the MS plots, the conduction band minimum (CBM) was determined to be −1.14 eV vs. NHE, and consequently, the valence band maximum (VBM) was calculated to be 1.14 eV vs. NHE (**Figure 3.2f**). The conduction band position of $CsPbBr_3$ is sufficiently negative to enable efficient electron transfer to the LUMO of the cobaloxime cocatalysts, thereby promoting charge separation. These photogenerated electrons sequentially reduce the cobalt center [$Co^{III} \rightarrow Co^{II} \rightarrow Co^{I}$] (**see later in the reaction mechanism, Figure 3.3e**).[39–41] The resulting electron-rich [Co^{I}] species initiates hydride formation, generating [$Co^{I}(H)_2$], which plays a crucial role in the hydrogen-borrowing mechanism, facilitating the hydrogenation of imines to amines (see later).

3.8. Optimization of reaction conditions

The photoredox N-alkylation reaction was optimized using benzyl alcohol (1) and aniline (2) as model substrates under visible-light irradiation in various solvents (**Table 3.2**). Among

them, toluene was the most effective solvent for C–N bond formation under a nitrogen atmosphere. No product formation was observed without $CsPbBr_3$ or light. Using bare $CsPbBr_3$ alone resulted in only 22% aniline conversion, with imine as the major product, exhibiting 83% selectivity for imine and just 17% for the amine. To improve the reaction, photocatalytic N-alkylation was further evaluated using various conventional semiconductors (TiO_2, C_3N_4, CdS, and $BiVO_4$) in combination with the [Co-4] cocatalyst under visible light (**Table 3.3a**). Among these, the $CsPbBr_3$ loaded with 5 wt.% [Co-4] (denoted $CsPbBr_3$–[Co-4]) exhibited superior performance, achieving 98% aniline conversion and 97% selectivity for N-benzylaniline (**Table 3.2**).

The N-alkylation of aniline with benzyl alcohol was also tested using various cocatalysts, including $Co(dmgH)_2$, $Ni(dmgH)_2$, and $Cu(dmgH)_2$ complexes (**Figure 3.3a**). Among the $Co(dmgH)_2$ derivatives ([Co-1] through [Co-4]), the $CsPbBr_3$–[Co-4] composite delivered the best performance, achieving 98% conversion and 97% selectivity for N-benzylamine. This result highlights the role of cobaloxime cocatalysts in facilitating the hydrogen borrowing process. Previous studies have also demonstrated that cobalt active sites are highly effective in such mechanisms. Additionally, the amount of cocatalyst was found to influence the photoredox activity significantly (**Table 3.2**). The optimal loading was 5 wt.% [Co-4], while higher loadings led to reduced activity. The N-alkylation reaction did not proceed when only the cocatalyst was used, under either dark or light conditions.

Mott–Schottky (MS) analysis confirmed that the CB of $CsPbBr_3$ is more negative than the LUMO of the cocatalysts, allowing efficient electron transfer from the CB to the cocatalyst. This electron transfer generates electron-rich cobalt active sites that promote cobalt–hydride bond formation during alcohol dehydrogenation. These findings confirm that the cocatalysts

Table 3.2. Optimization of *N*-alkylation of aniline with benzyl alcohol under different conditions.

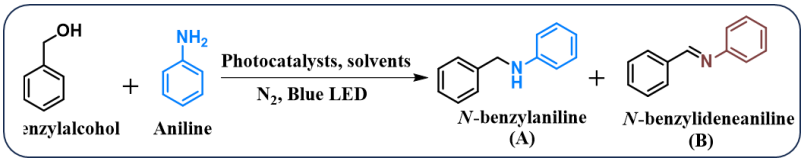

S. N.	Photocatalyst	Solvent	Conv. (%)	selectivity (%) **(A)**	selectivity (%) **(B)**
Photocatalysts variation					
1	$CsPbBr_3$ QDs	Toluene	22	17	83
2	$CsPbBr_3$-[Co-1]	Toluene	78	61	39
3	$CsPbBr_3$-[Co-2]	Toluene	80	73	27
4	$CsPbBr_3$-[Co-3]	Toluene	97	90	10
5	**$CsPbBr_3$-[Co-4]**	**Toluene**	**98**	**97**	**3**
Variation of wt.% [Co-4] **cocatalyst**					
6	$CsPbBr_3$-[Co-4] 3 wt.%	Toluene	91	95	5
7	**$CsPbBr_3$-[Co-4] 5 wt.%**	**Toluene**	**98**	**97**	**3**
8	$CsPbBr_3$-[Co-4] 7 wt.%	Toluene	96	98	2
Variation of solvents					
9	$CsPbBr_3$-[Co-4]	Acetonitrile	76	91	9
10	$CsPbBr_3$-[Co-4]	Tetrahydrofuran	59	88	12
11	**$CsPbBr_3$-[Co-4]**	**Toluene**	**98**	**97**	**3**
12	$CsPbBr_3$-[Co-4]	1,4-Dioxane	83	82	18
Other variations in the reaction conditions					
13	-	Toluene	ND	ND	ND
14	[Co-4]	Toluene	ND	ND	ND
15	$CsPbBr_3$-[Co-4]	Toluene/ dark	trace	trace	Trace

Reaction conditions: aniline (0.5 mmol), benzyl alcohol (0.8 mmol), catalyst (10 mg), solvent (2.0 mL), irradiated with a 15 W blue LED at 33 ± 3 °C for 17 hours. After completion, the photocatalyst was recovered by centrifugation at 15,000 rpm for 10 minutes. The product was purified by silica gel column chromatography using varying ratios of ethyl acetate and hexane. Product formation and purity were confirmed by ^{1}H and ^{13}C NMR spectroscopy. Isolated yield is reported.

play a crucial role in enhancing both the activity and selectivity of the N-alkylation of aniline.

The quenching experiments further confirmed the involvement of photogenerated electrons and holes in initiating the reaction. Various scavengers were employed to investigate

the photocatalytic N-alkylation of aniline with benzyl alcohol over $CsPbBr_3$–[Co-4].[42] $AgNO_3$ and TEOA were used as electron and hole scavengers, respectively. A marked decrease in product yield upon their addition indicated the essential role of electron–hole pairs in the reaction (**Figure 3.3c**). The electron scavenger ($AgNO_3$) blocked CB electron transfer to the cocatalyst, while the hole scavenger (TEOA) suppressed benzylalcohol oxidation at the VB. Additionally, the use of tert-butyl alcohol (TBA) confirmed that hydroxyl radicals ($^{\bullet}OH$) were not involved in the N-alkylation process. Interestingly, the formation of a benzylic radical intermediate (4b) was verified by trapping it with TEMPO, and the resulting adduct was characterized via mass spectrometry.

3.9. Reaction mechanism

The outstanding performance of the $CsPbBr_3$–[Co-4] composite in the N-alkylation of aniline with benzyl alcohol prompted (**Figure 3.3d**) further investigation into the underlying catalytic mechanism (**Figure 3.3e**).[43] Photoredox N-alkylation of amines via the borrowing hydrogen strategy remains particularly challenging, as it involves the oxidation of benzyl alcohol followed by a complex multi-step process. Notably, $CsPbBr_3$–[Co-4] enables efficient tandem alcohol oxidation, achieving high selectivity for amine formation. Upon blue LED irradiation, the $CsPbBr_3$ QDs generate electron–hole pairs, with photogenerated electrons (e^-) and holes (h^+) separated across the QD surface.[44–46] The CB electrons can undergo two-electron transfer (SET) to the cobaloxime cocatalyst, generating electron-rich cobalt species, a thermodynamically favourable process. This enables cobalt to cycle through redox states (Co^{III} → Co^{II} →Co^{I}) during the reaction (**Figure 3.3e**).[46–49] Simultaneously, the VB of $CsPbBr_3$ is sufficiently positive to thermodynamically oxidize benzyl alcohol, initiating the dehydrogenation step. The photogenerated holes oxidize surface-adsorbed benzyl alcohol to

benzaldehyde, releasing two hydrogen atoms that are transferred to the electron-rich [Co^{I}] sites, leading to the formation of cobalt–hydride ([Co–H]) active species.[50–53] Subsequently, the in situ–generated benzaldehyde condenses with aniline to form the imine intermediate N-benzylideneaniline (**4a**), which is then selectively hydrogenated by [Co–H], yielding the final product, N-benzylaniline (**3a**), and regenerating the [Co^{III}] species to complete the catalytic cycle (**Figure 3.3e**). This strongly suggests that the reaction proceeds via a "borrowing hydrogen" or "transfer hydrogenation" mechanism facilitated by the [Co-4] cocatalyst, with benzyl alcohol dehydrogenation being the key step that governs the N-alkylation process.

3.10. Control study of *N*-Alkylation of aniline

In this study, the N-alkylation reaction proceeds through two key steps: (i) the dehydrogenation

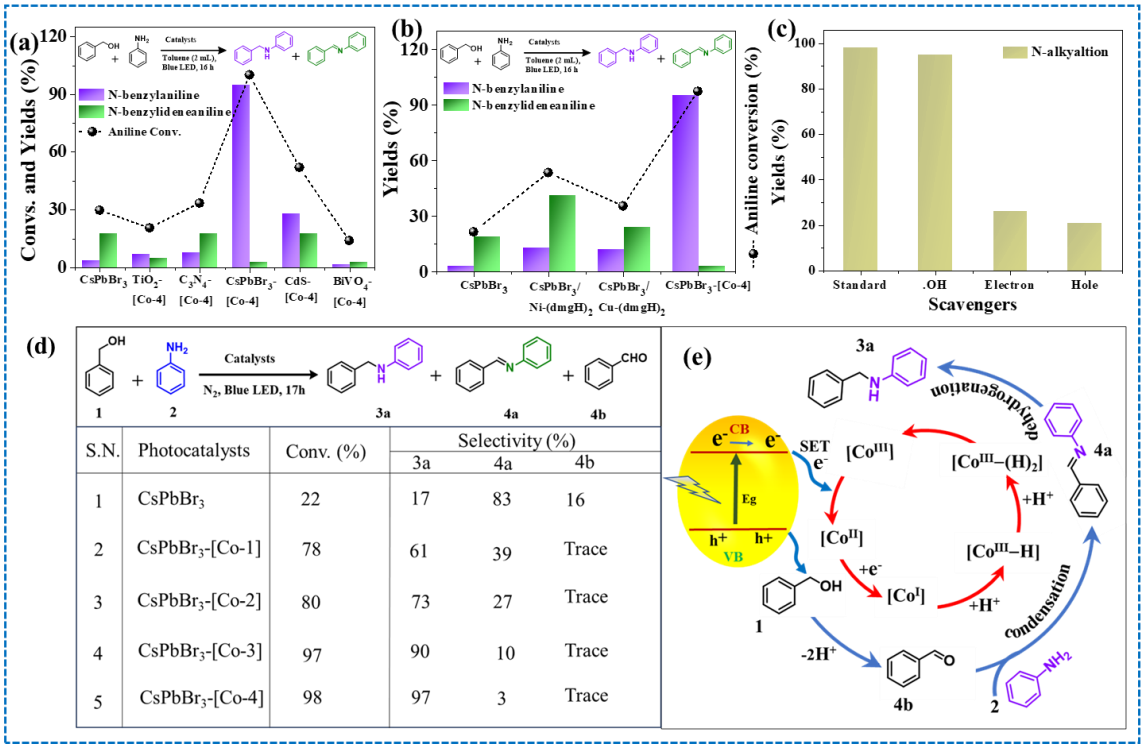

S.N.	Photocatalysts	Conv. (%)	Selectivity (%)		
			3a	4a	4b
1	$CsPbBr_3$	22	17	83	16
2	$CsPbBr_3$-[Co-1]	78	61	39	Trace
3	$CsPbBr_3$-[Co-2]	80	73	27	Trace
4	$CsPbBr_3$-[Co-3]	97	90	10	Trace
5	$CsPbBr_3$-[Co-4]	98	97	3	Trace

Figure 3.3. (a) N-alkylation activity over different photocatalysts with [Co-4]. (b) N-alkylation activity over $CsPbBr_3$ with different cocatalysts. (c) Quenching experiments. (d) The optimization of N-alkylation of aniline with benzylalcohol. (e) Proposed mechanism of N-alkylation reaction over $CsPbBr_3$-[Co-4] catalyst. **Reaction condition:** 0.5 mmol (aniline), 0.8 mmol benzylalcohol, 10 mg catalyst, 2 mL toluene, 17 h under blue LED irradiation.

of alcohol and (ii) hydrogen transfer from the cobalt–hydride species to the imine intermediate. Kinetic studies of various cocatalyst (Co-1, Co-2, Co-3, and Co-4) combinations with $CsPbBr_3$ revealed their influence on the rate of benzyl alcohol dehydrogenation to benzaldehyde (**Figure 3.4a**). The oxidation of benzyl alcohol is driven by photogenerated holes, and this step is directly linked to the efficiency of charge separation within the $CsPbBr_3$. All tested cocatalysts impacted charge separation to varying degrees, with $CsPbBr_3$–[Co-4] exhibiting the most efficient charge separation and the highest benzaldehyde yield. In contrast, bare $CsPbBr_3$ gave only moderate yields, underscoring the crucial role of the cocatalyst in enhancing dehydrogenation and accelerating reaction rates.

To investigate the hydrogen atom transfer from the [Co–H] system and the subsequent hydrogenation of N-benzylideneaniline to N-benzylaniline for all the catalysts **(Figure 3.4b)**. In addition, benzyl alcohol and aniline are taken as a model substrate and tested over all the catalysts. Initially, benzyl alcohol undergoes dehydrogenation at the VB of $CsPbBr_3$, generating benzaldehyde and two hydrogen atoms. These hydrogens combine with electrons transferred to the cobalt cocatalyst to form [Co–H] species. The [Co–H] then facilitates hydrogen transfer to the imine intermediate, N-benzylideneaniline, yielding the final product, N-benzylaniline. The efficiency of this hydrogen transfer is strongly influenced by the electronic environment around the cobalt active site. Among all tested catalysts, [Co-4] showed the highest activity, attributed to increased steric crowding at the equatorial position of the cobalt centre, induced by the 2,3-Naphthalenediamine ligand. This steric effect enhances hydrogenation efficiency, resulting in 98% conversion and 97% selectivity.

In comparison, $CsPbBr_3$ alone exhibited only moderate conversion (**Figure 3.4b**). The [Co-4] cocatalyst electronic environment manipulated by the steric crowding 2,3-

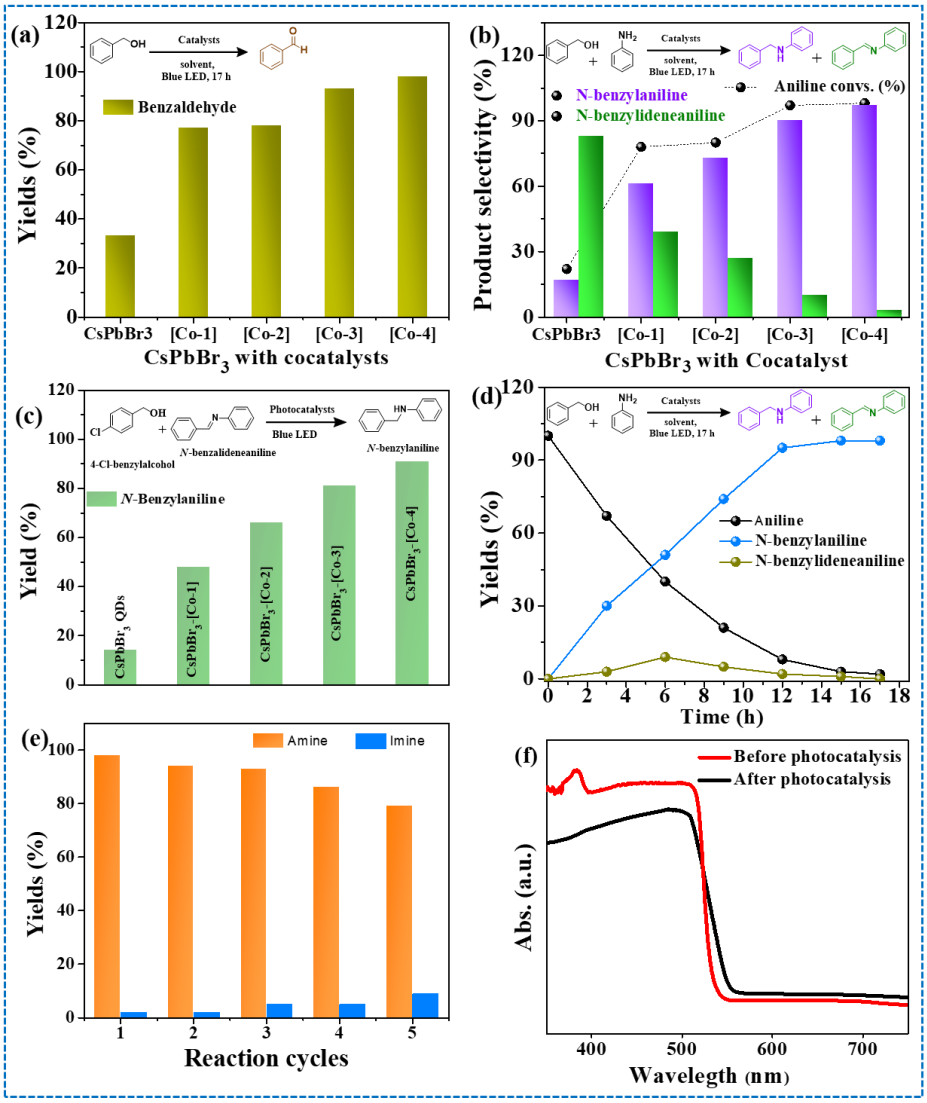

Figure 3.4. (a) The optimization rate of the dehydrogenation of benzylalcohol. (b) The selectivity of the N-alkylation reaction over all the catalysts. (c) Model reactions illustrating the strong hydrogen atom transfer ability of $CsPbBr_3$-[Co-4]. (d) Time-dependent reaction of N-alkylation of amine over $CsPbBr_3$-[Co-4]. (e) Recyclability test. (f) Comparison of UV-DRS before and after the photocatalyst.

napthalendiamine ligand facilitates the hydrogen transfer.

Additionally, alcohol was confirmed to act as a hydrogen source, as demonstrated by the reaction between N-benzylideneaniline and 4-chlorobenzyl alcohol, which yielded N-benzylaniline (**Figure 3.4c**). In contrast, performing the same reaction over $CsPbBr_3$ alone resulted in only 14% conversion to N-benzylaniline, indicating limited hydrogenation

capability. Notably, $CsPbBr_3$–[Co-4] exhibited the highest hydrogenation efficiency, achieving 91% conversion to N-benzylaniline, significantly outperforming $CsPbBr_3$–[Co-1], $CsPbBr_3$–[Co-2], and $CsPbBr_3$–[Co-3] (**Figure 3.4c**).

Time-dependent conversion of aniline and product formation during the N-alkylation reaction over $CsPbBr_3$–[Co-4] was investigated (**Figure 3.4d**). The results revealed that aniline conversion increased with irradiation time, reaching nearly 98% after 17 hours. In contrast, the intermediate **4a** initially accumulated, peaking at 6 hours before decreasing, indicating that 4a serves as an intermediate in the reaction. As the reaction progressed, the yield of N-benzylaniline (**3a**) steadily increased, while the yield of N-benzylideneaniline decreased, reflecting the gradual hydrogenation of the imine to the amine (**Figure 3.4d**). When aniline conversion reached 98%, only trace amounts of the imine (N-benzylideneaniline) were observed. These results confirm that the N-alkylation reaction between aniline and benzyl alcohol, under $CsPbBr_3$–[Co-4] irradiation, proceeds via **4a** as an intermediate. Furthermore, product selectivity is influenced by the cocatalyst's ability to mediate hydride transfer from the cobalt–hydride species to the imine intermediate (N-benzylideneaniline). The [Co-4] cocatalyst, featuring a strongly conjugated 2,3-diphenylamine ligand, enhances this transfer due to its more electron-deficient cobalt centre, thereby facilitating efficient hydrogenation.

The catalyst stability was assessed through recycling experiments. After five reaction cycles, the conversion of aniline remained above 80%, and product selectivity stayed above 88% (**Figure 3.4e**). The slight decrease in activity after the second cycle was primarily attributed to physical loss of the catalyst during transfer, as no significant changes were observed in the UV absorption spectra (**Figure 3.4f**).

3.11. Substrate scope of amine formation

Under optimized conditions, various alcohols were evaluated for the N-alkylation of anilines (**Table 3.3**), showing broad substrate scope and good functional group tolerance. Electron-donating substituents (e.g., methoxy, methyl) enhanced reactivity; 4-methoxybenzyl alcohol gave 96% yield (**Table 3.3, 3b**), and 4-methylbenzyl alcohol outperformed benzyl alcohol (**Table 3.3, 3c**). Steric hindrance at ortho or para positions further improved the product yields (**Table 3.3, 3d**). In contrast, electron-withdrawing groups at benzyl alcohol, like chloro and bromo, produced slightly lowered product yields (**Table 3.3, 3e-3f**). Benzyl alcohol also reacted with various substituted anilines (**Table 3.3, 3g-3i**); electron-withdrawing groups on anilines reduced yields, 4-fluoro (89%, **Table 3.3, 3g**), 4-chloro (90%, **Table 3.3, 3h**), and 2,4,5-trichloroaniline gave the lowest yield (87%, **Table 3.3, 3i**), likely due to steric effects.

Notably, the presence of electron-donating group at benzyl alcohol and aniline significantly improved the product yield to 95% (**Table 3.3, 3j**), and with 4-methylaniline, 98% (**Table 3.3, 3k**). Pairing 4-methoxybenzyl alcohol with 4-methoxyaniline yielded 91%, slightly lower due to the mesomeric effect (**Table 3.3, 3l**). Yield trends correlated with alcohol dehydrogenation at the $CsPbBr_3$ valence band, where electron-rich alcohols, acting as hole scavengers, enhanced interaction with photo-generated holes, boosting yields. Conversely, electron-withdrawing groups weakened this interaction, reducing efficiency. Heterocyclic alcohols like 2-pyridinemethanol and 2-thiophenemethanol gave 92% and 86% with aniline (**Table 3.3, 3m–3n**), while heteroaromatic anilines with benzyl alcohol also performed well, reaching up to 90% yield (**Table 3.3, 3o**), and all products were characterized by NMR spectroscopy **(Table 3.4)**.

Table 3.3. The substrate scope of *N*-alkylation of amines.

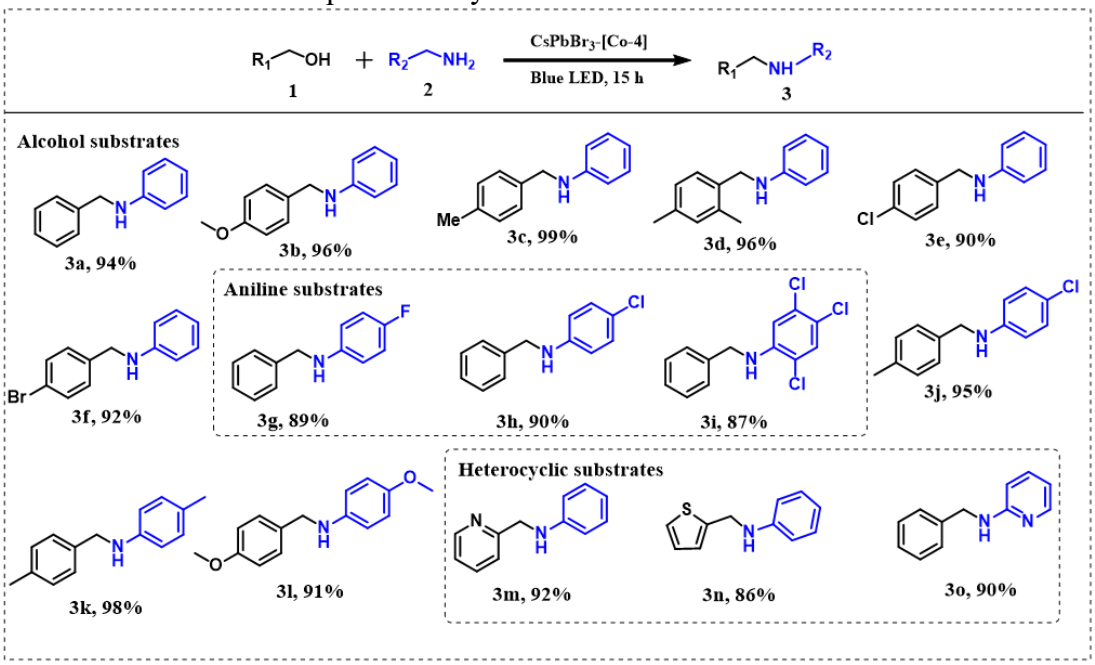

Reaction conditions: Alcohols (0.8 mmol), amines (0.5 mmol), $CsPbBr_3$-[Co-4] (10 mg), Toluene (2 mL), 15 W Blue LED, temperature: 35 ± 3 °C, Time: 15 h. In all cases, the isolated yields of the products were reported, and the products were characterized using ^{1}H and ^{13}C NMR spectroscopy (Table 3.4).

3.12. Conclusion

In summary, we demonstrated that $CsPbBr_3$ QDs effectively catalyse the photoredox N-alkylation of amines with alcohols under visible light. The incorporation of cobaloxime cocatalysts significantly enhances the catalytic performance by improving charge separation and promoting alcohol oxidation to aldehydes. The cocatalysts also govern product selectivity through hydrogen atom transfer (borrowing hydrogen) from the [Co–H] species. Subsequent condensation of the aldehyde with amine yields N-benzylideneaniline. Among the tested cocatalysts, [Co-4] exhibited superior activity due to its favourable LUMO energy and strong ligand conjugation at the equatorial position, achieving 97% selectivity. This photocatalytic system operates under mild conditions without the need for external hydrogen sources, bases, or elevated temperatures, highlighting the potential of $CsPbBr_3$ in the sustainable synthesis of

valuable amine compounds.

Table 3.4. Characterization of the products by ^{1}H NMR and ^{13}C NMR spectroscopy[1,19,43]

3a: N-benzylaniline 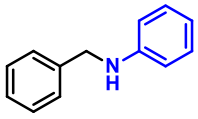	^{1}H NMR (500 MHz, $CDCl_3$) δ: 7.42 (dd, J = 13.0, 6.0 Hz, 4H), 7.35 (d, J = 6.0 Hz, 1H), 7.25 (t, J = 7.2 Hz, 2H), 6.79 (t, J = 6.8 Hz, 1H), 6.71 (d, J = 7.8 Hz, 2H), 4.39 (s, 2H), 3.84 (s, 1H). ^{13}C NMR (125 MHz, $CDCl_3$) δ: 148.22, 139.51, 129.35, 128.72, 127.59, 127.31, 117.59, 112.88, 48.37. **Yield: 94%, 94 mg, and 0.47 mmol**
3b: N-(4-methoxybenzyl)aniline 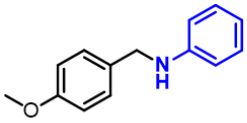	^{1}H NMR (500 MHz, $CDCl_3$) δ: 7.28 (d, J = 8.6 Hz, 2H), 7.17 (t, J = 7.9 Hz, 2H), 6.87 (d, J = 8.6 Hz, 2H), 6.71 (t, J = 7.3 Hz, 1H), 6.63 (d, J = 7.7 Hz, 2H), 4.24 (s, 2H), 3.79 (s, 3H). ^{13}C NMR (125 MHz, $CDCl_3$) δ: 158.89, 148.17, 131.40, 129.28, 128.85, 117.58, 114.05, 112.92, 55.32, 47.85. **Yield: 96%, 110 mg, and 0.48 mmol**
3c: N-(4-methylbenzyl)aniline 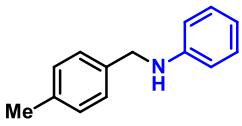	^{1}H NMR (500 MHz, $CDCl_3$) δ: 7.31 (d, J = 5.4 Hz, 2H), 7.21 (d, J = 5.0 Hz, 4H), 6.73 (dd, J = 39.7, 4.5 Hz, 3H), 4.33 (d, J = 2.8 Hz, 2H), 4.03 (s, 1H), 2.40 (s, 3H). ^{13}C NMR (125 MHz, $CDCl_3$) δ: 148.28, 136.93, 136.42, 129.35, 127.59, 117.49, 112.84, 48.12, 21.15. **Yield: 99%, 103 mg, and 0.49 mmol**
3d: N-(2,4-dimethylbenzyl)aniline 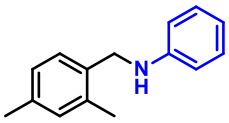	^{1}H NMR (500 MHz, $CDCl_3$) δ: 7.48 – 7.38 (m, 4H), 7.35 (t, J = 6.6 Hz, 1H), 6.98 (s, 2H), 6.60 (d, J = 7.7 Hz, 1H), 4.42 (s, 2H), 3.80 (s, 1H), 2.30 (s, 3H), 2.22 (s, 3H). ^{13}C NMR (126 MHz, $CDCl_3$) δ: 143.88, 139.79, 131.07, 128.70, 127.52, 127.45 127.24, 126.37, 122.15, 110.20, 48.62, 20.46, 17.59. **Yield: 96%, 109 mg, and 0.47 mmol**
3e: N-(4-chlorobenzyl)aniline 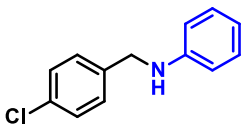	^{1}H NMR (500 MHz, $CDCl_3$) δ: 7.33 (m, 4H), 7.20 (dd, J = 8.5, 7.4 Hz, 2H), 6.76 (t, J = 7.3 Hz, 1H), 6.64 (d, J = 7.6 Hz, 2H), 4.34 (s, 2H), 4.30 (s, 1H). ^{13}C NMR (125 MHz, $CDCl_3$) δ: 147.84, 138.01, 132.88, 129.33, 128.77, 128.72, 117.78, 112.85, 47.62. **Yield: 90%, 105 mg, and 0.45 mmol**
3f: N-(4-bromobenzyl)aniline 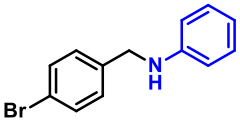	^{1}H NMR (500 MHz) δ: 7.44 – 7.38 (m, 4H), 7.35 (s, 1H), 7.30 (d, J = 8.9 Hz, 2H), 6.55 (d, J = 8.9 Hz, 2H), 4.34 (s, 2H), 4.13 (s, 1H). ^{13}C NMR (125 MHz, $CDCl_3$) δ: 147.13, 138.95, 132.01, 128.80, 127.48, 114.56, 114.51, 109.14, 48.26.

	Yield: 92%, 128 mg, and 0.45 mmol
3g: N-benzyl-4-fluoroaniline 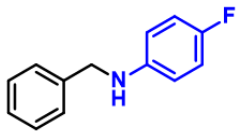	^{1}H NMR (500 MHz, $CDCl_3$) δ: 7.41 (dd, J = 5.3, 2.6 Hz, 4H), 7.36 – 7.32 (m, 1H), 6.96 – 6.90 (m, 2H), 6.61 (dd, J = 9.0, 4.4 Hz, 2H), 4.34 (s, 2H), 3.98 (s, 1H). ^{13}C NMR (125 MHz, $CDCl_3$) δ: 156.85 (d, J_{C-F} = 233.0 Hz), 154.98, 144.54, 139.29, 128.73, 127.54, 115.78 (d, J_{C-F} = 15.3 Hz), 113.67 (d, J_{C-F} = 2.7 Hz), 48.94.s **Yield: 89%, 97 mg and 0.44 mmol**
3h: N-benzyl-4-chloroaniline 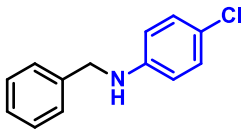	^{1}H NMR (500 MHz, $CDCl_3$) δ: 7.39 (d, J = 4.4 Hz, 4H), 7.33 (d, J = 4.6 Hz, 1H), 7.15 (d, J = 8.8 Hz, 2H), 6.58 (d, J = 8.9 Hz, 2H), 4.34 (s, 2H), 4.09 (s, 1H). ^{13}C NMR (125 MHz, CDCl3) δ: 146.66, 138.95, 129.11, 128.74, 127.45, 122.11, 113.94, 48.35. **Yield: 90%, 105 mg, and 0.45 mmol**
3i: N-benzyl-2,4,5-trichloroaniline 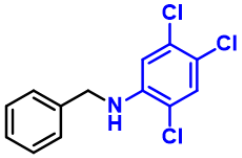	^{1}H NMR (500 MHz, $CDCl_3$) δ 7.42 – 7.31 (m, 6H), 6.70 (s, 1H), 4.75 (s, 1H), 4.37 (s, 2H). ^{13}C NMR (125 MHz, $CDCl_3$) δ: 137.65, 131.77, 129.93, 129.01, 127.85, 127.40, 119.50, 117.83, 112.30, 47.94. **Yield: 87%, 132 mg and 0.43 mmol**
3j: 4-chloro-N-(4-methylbenzyl)aniline 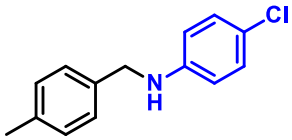	^{1}H NMR (500 MHz, $CDCl_3$) δ: 7.31 – 7.25 (m, 4H), 7.18 (d, J = 7.9 Hz, 2H), 6.61 – 6.50 (m, 2H), 4.28 (s, 2H), 4.07 (s, 1H), 2.38 (s, 3H). ^{13}C NMR (125 MHz, $CDCl_3$) δ: 147.13, 137.09, 135.80, 131.94, 129.41, 127.44, 114.38, 109.03, 48.00, 21.12. **Yield: 95%, 118 mg and 0.47 mmol**
3k: 4-methyl-N-(4-methylbenzyl)aniline 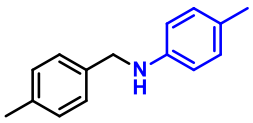	^{1}H NMR (500 MHz, $CDCl_3$) δ: 7.30 (t, J = 9.0 Hz, 2H), 7.20 (d, J = 7.9 Hz, 2H), 7.04 (d, J = 8.4 Hz, 2H), 6.62 (d, J = 8.3 Hz, 2H), 4.31 (s, 2H), 3.90 (s, 1H), 2.40 (s, 3H), 2.30 (s, 3H). ^{13}C NMR (125 MHz, $CDCl_3$) δ: 146.04, 136.82, 136.62, 129.81, 129.32, 127.56, 126.71, 112.98, 48.44, 21.20, 20.48. **Yield: 98%, 112 mg and 0.49 mmol**
3l: 4-methoxy-N-(4-methoxybenzyl)aniline 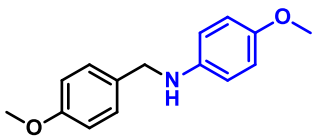	^{1}H NMR (500 MHz, $CDCl_3$) δ: 7.32 (d, *J* = 8.6 Hz, 2H), 6.91 (d, *J* = 8.6 Hz, 2H), 6.81 (d, *J* = 8.9 Hz, 2H), 6.64 (d, *J* = 8.9 Hz, 2H), 4.24 (s, 2H), 3.83 (s, 3H), 3.77 (s, 3H). ^{13}C NMR (126 MHz, $CDCl_3$) δ: 159.11, 152.46, 142.83, 131.97, 129.13, 115.20, 114.36, 56.11, 55.59, 49.03. **Yield: 91%, 119 mg, and 0.45 mmol**

3m: N-benzylpyridin-2-amine 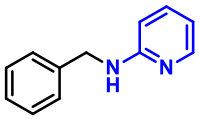	^{1}H NMR (500 MHz, $CDCl_3$) δ: 8.12 (d, J = 5.0 Hz, 1H), 7.45 – 7.34 (m, 5H), 7.32 – 7.28 (m, 1H), 6.65 – 6.57 (m, 1H), 6.39 (d, J = 8.4 Hz, 1H), 5.07 (s, 1H), 4.53 (d, J = 5.4 Hz, 2H). ^{13}C NMR (125 MHz, $CDCl_3$) δ: 158.65, 148.19, 139.17, 137.56, 128.67, 127.34, 113.12, 106.77, 46.34. **Yield: 90%, 90 mg and 0.45 mmol**
3n: N-(thiophen-2-ylmethyl)aniline 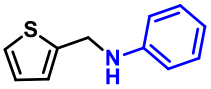	^{1}H NMR (500 MHz, $CDCl_3$) δ: 8.61 (d, J = 5.5 Hz, 1H), 7.67 (d, J = 1.7 Hz, 1H), 7.37 (d, J = 7.8 Hz, 1H), 7.27 – 7.10 (m, 4H), 6.75 (t, J = 7.3 Hz, 1H), 6.70 (d, J = 8.6 Hz, 2H), 4.49 (s, 2H), 4.25 (s, 1H). ^{13}C NMR (125 MHz, $CDCl_3$) δ:158.56, 149.19, 147.88, 136.72, 129.27, 122.16, 121.65, 117.58, 113.02, 49.28. **Yield: 92%, 93 mg, and 0.46 mmol**
3o: N-(pyridin-2-ylmethyl)aniline 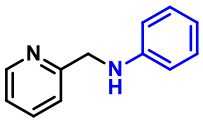	1H NMR (500 MHz, CDCl3) δ 7.28 – 7.18 (m, 3H), 7.05 (dd, J = 3.4, 1.1 Hz, 1H), 7.00 (dd, J = 5.1, 3.5 Hz, 1H), 6.78 (t, J = 7.3 Hz, 1H), 6.74 – 6.67 (m, 2H), 5.32 (s, 2H), 4.54 (s, 1H). ^{13}C NMR (125 MHz, $CDCl_3$) δ:147.84, 138.65, 129.52 – 128.67, 125.84, 124.69, 122.50, 118.27, 114.33 – 113.84, 43.03. **Yield: 86%, 89 mg, and 0.43 mmol**

3.13. ^{1}H NMR and ^{13}C NMR spectra of the compound

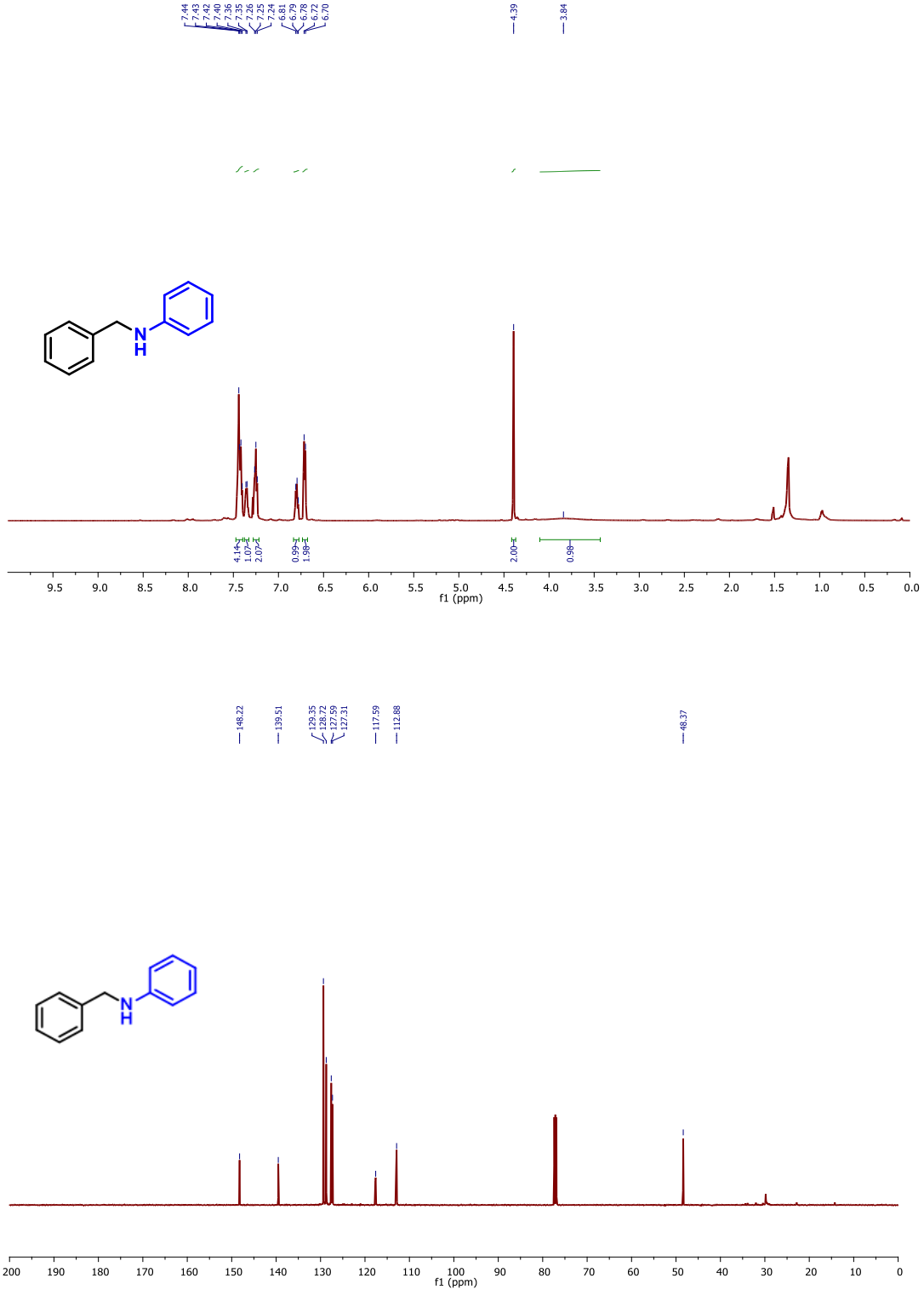

Figure 3.5. ^{1}H NMR and ^{13}C NMR spectra of the compound **3a.**

3.14. Reference

1 J. He, B. Han, C. Xian, Z. Hu, T. Fang, and Z. Zhang, 2024. *Angew. Chem. Int. Edt.*, ***63***, 202404515.

2 J. Magano and J. R. Dunetz, *RSC Catal. Ser*, 2015, **40**, 697–778.

3 F. Monnier and M. Taillefer, *Angew. Chemie - Int. Ed.*, 2008, **47**, 3096–3099.

4 M. T. Pirnot, Y.M. Wang and S. L. Buchwald, *Angew. Chem. Int. Ed.*, 2016, **55**, 48–57.

5 S. K. Nimmagadda, S. Kalidindi, S. S. Bondigela, S. Korapati, D. Dasgupta, N. A. Malik, P. Rao, P. Maity, J. R. Coombs, M. Hay, E. M. Simmons, S. Mukherjee, R. Vaidyanathan, M. D. Eastgate and F. González-Bobes, *Org. Process Res. Dev.*, 2024, **28**, 3414–3422.

6 M. R. Ball, T. S Wesley, K. R. Rivera-Dones, G. W. Huber, and J. A. Dumesic, *Green Chem*. 2018, **20**, 4695−4709

7 T. Wang, J. Ibañez, K. Wang, L. Fang, M. Sabbe, C. Michel, S. Paul, M. Pera-titus and P. Sautet, 2019, **2**, 773-779.

8 A. Corma, J. Navas and M. J. Sabater, *Chem. Rev.*, 2018, **118**, 1410–1459.

9 K. Zhang, Y. Huang, D. Zhang, J. Wu, Y. Mai, N. Cai, C. Wang, H. Yue, W. Liang and R. Su, *Chem. - A Eur. J.*, 2024, **30**, 202401540.

10 Z. Chi, J. Bin Liao, X. Cheng, Z. Ye, W. Yuan, Y. M. Lin and L. Gong, *J. Am. Chem. Soc.*, 2024, **146**, 10857–10867.

11 M. H. S. A. Hamid, C. L. Allen, G. W. Lamb, A. C. Maxwell, H. C. Maytum, A. J. A. Watson and J. M. J. Williams, *J. Am. Chem. Soc.*, 2009, **131**, 1766–1774.

12 G. Zou, R. Cao, C. Cui, Y. Luo, C. Huang, X. Cui, Z. Wang and Y. Song, *Catal. Sci. Technol.*, 2023, **13**, 3916–3926.

13 J. J. A. Celaje, X. Zhang, F. Zhang, L. Kam, J. R. Herron and T. J. Williams, *ACS Catal.*, 2017, **7**, 1136–1142.

14 H. Liu, D. L. Wang, X. Chen, Y. Lu, X. L. Zhao and Y. Liu, *Green Chem.*, 2017, **19**, 1109–1116.

15 R. Kawahara, K. I. Fujita and R. Yamaguchi, *J. Am. Chem. Soc.*, 2010, **132**, 15108–15111.

16 C. K. Prier, D. A. Rankic and D. W. C. MacMillan, *Chem. Rev.*, 2013, **113**, 5322–5363.

17 N. A. Till, L. Tian, Z. Dong, G. D. Scholes and D. W. C. MacMillan, *J. Am. Chem. Soc.*, 2020, **142**, 15830–15841.

18 S. Song, J. Qu, P. Han, M. J. Hülsey, G. Zhang, Y. Wang, S. Wang, D. Chen, J. Lu and N. Yan, *Nat. Commun.*, 2020, **11**, 4899.

19 Y. Yuan, J. Wang, H. Liu and Z. Li, *J. Mater. Chem. A*, 2023, **11**, 24127–24135.

20 S. Bera, A. Tripathi, T. Titus, N. M. Sethi, R. Das, N. Afreen, K. V. Adarsh, K. G. Thomas and N. Pradhan, *J. Am. Chem. Soc.*, 2024, **146**, 20300–20311.

21 X. Zhu, Y. Lin, J. San Martin, Y. Sun, D. Zhu and Y. Yan, *Nat. Commun.*, 2019, **10**,

4279.
22 Y. Xu, R. Chen, Z. Li, A. Li, H. Han and C. Li, *ACS Appl. Mater. Interfaces*, 2017, **9**, 23230–23237.
23 X. Wang, Y. Li and X. Wu, *ACS Catal.*, 2022, **12**, 3710–3718.
24 S. L. Meng, C. Zhang, C. Ye, J. H. Li, S. Zhou, L. Zhu, X. B. Li, C. H. Tung and L. Z. Wu, *Energy Environ. Sci.*, 2023, **16**, 1590–1596.
25 S. Shibutani, K. Nagao and H. Ohmiya, *J. Am. Chem. Soc.*, 2024, **146**, 4375–4379.
26 H. L. Sun, F. Yang, W. T. Ye, J. J. Wang and R. Zhu, *ACS Catal.*, 2020, **10**, 4983–4989.
27 K. Zhuang, G. C. Haug, Y. Wang, S. Yin, H. Sun, S. Huang, R. Trevino, K. Shen, Y. Sun, C. Huang, B. Qin, Y. Liu, M. Cheng, O. V. Larionov and S. Jin, *J. Am. Chem. Soc.*, 2024, **146**, 8508–8519.
28 F. Xu, K. Meng, B. Cheng, S. Wang, J. Xu and J. Yu, *Nat. Commun.*, 2020, **11**, 4613.
29 Z. Zhang, L. Li, Y. Jiang and J. Xu, *Inorg. Chem.*, 2022, **61**, 3351–3360.
30 V. Kumar, S. K. Patel, V. Vyas, D. Kumar, E. S. Subramaniam Iyer and A. Indra, *Chem. Sci.*, 2024, **15**, 13218–13226.
31 Y. Dong, Y. Feng, Z. Li, H. Zhou, H. Lv and G.-Y. Yang, *ACS Catal.*, 2023, **13**, 14346–14355.
32 İ. Özçeşmeci, A. Demir, D. Akyüz, A. Koca and A. Gül, *Inorganica Chim. Acta*, 2017, **466**, 591–598.
33 A. Paik, C. Das, S. Paul, A. Biswas, S. Mehta, A. Mondal, B. Maity, A. Dutta and S. Rana, *ACS Catal.*, 2024, 15498–15513.
34 D. Basu, S. Mazumder, J. Niklas, H. Baydoun, D. Wanniarachchi, X. Shi, R. J. Staples, O. Poluektov, H. B. Schlegel and C. N. Verani, *Chem. Sci.*, 2016, **7**, 3264–3278.
35 S. U. Dighe, F. Juliá, A. Luridiana, J. J. Douglas and D. Leonori, *Nature*, 2020, **584**, 75–81.
36 S. T. Gebre, L. M. Kiefer, F. Guo, K. R. Yang, C. Miller, Y. Liu, C. P. Kubiak, V. S. Batista and T. Lian, *J. Am. Chem. Soc.*, 2023, **145**, 3238–3247.
37 W. Song, K. C. Chong, G. Qi, Y. Xiao, G. Chen, B. Li, Y. Tang, X. Zhang, Y. Yao, Z. Lin, Z. Zou and B. Liu, *J. Am. Chem. Soc.*, 2024, **146**, 3303–3314.
38 H. Huang, D. Verhaeghe, B. Weng, B. Ghosh, H. Zhang, J. Hofkens, J. A. Steele and M. B. J. Roeffaers, *Angew. Chem. Int. Ed.*, 2022, **134**, 202203261.
39 M. Shamsipur, A. Salimi, H. Haddadzadeh and M. F. Mousavi, *J. Electroanal. Chem.*, 2001, **517**, 37–44.
40 J. C. Manton, C. Long, J. G. Vos and M. T. Pryce, *Dalt. Trans.*, 2014, **43**, 3576–3583.
41 P. Dam, K. Zuo, L. M. Azofra and O. El-Sepelgy, *Angew. Chem. Int. Edt.*, , 2024,**136,** 202405775.
42 M. Hao, X. Deng, L. Xu and Z. Li, *Appl. Catal. B Environ.*, 2019, **252**, 18–23.
43 F. Niu, W. Tu, X. Lu, H. Chi, H. Zhu, X. Zhu, L. Wang, Y. Xiong, Y. Yao, Y. Zhou and Z. Zou, *ACS Catal.*, 2022, **12**, 4481–4490.

44 J.L. Dempsey, J.R. Winkler and H.B. Gray, *J. Am. Chem. Soc.*, 2010, **132**,16774-16776.

45 D.P. Estes, D.C. Grills, and J.R. Norton, *J. Am. Chem. Soc.*, 2014, **136**, 17362-17365.

46 D.C. Lacy, G.M. Roberts, and J.C. Peters, *J. Am. Chem. Soc.*, 2015, **137**, 4860-4864.

47 Q. Cao, J. Feng, K.T. Chang, W. Liang, and H. Lu, *Adv. Materials*, 2025, **37**, 2409096.

48 N.Y. Huang, Y.T. Zheng, D. Chen, Z.Y. Chen, C.Z. Huang, and Q. Xu, *Chem. Soc. Reviews*, 2023, **52**, 7949-8004.

49 J. L. Dempsey, B. S. Brunschwig, J. R. Winkler and H. B. Gray, *Acc. Chem. Res.*, 2009, **42**, 1995–2004.

50 J. Li, C. Y. Huang, J. T. Han and C. J. Li, *ACS Catal.*., 2021, **11**, 14148–14158.

51 B.H. Solis, and S. Hammes-Schiffer, *J. Am. Chem. Soc.*, 2011, **133**, 19036-19039.

52 L. Huang, T. Ji, C. Zhu, H. Yue, N. Zhumabay, and M. Rueping, *Nat. Commun.*, 2022, **13**, 809.

53 J. Li, C.Y. Huang, J.T. Han, and C.J. Li, *ACS Catalysis*, 2021, **11**,14148-14158.